International Journal of Pharmaceutics 430 (2012) 216–227

Contents lists available at SciVerse ScienceDirect

International Journal of Pharmaceutics

journal homepage: www.elsevier.com/locate/ijpharm

Pharmaceutical nanotechnology

Solid lipid nanoparticles as intracellular drug transporters: An investigation of the uptake mechanism and pathway

S. Martins[a,*], S. Costa-Lima[b], T. Carneiro[a], A. Cordeiro-da-Silva[b,c], E.B. Souto[d,e], D.C. Ferreira[a]

[a] Laboratory of Pharmaceutical Technology/Centre of Research in Pharmaceutical Sciences (LTF/CICF), Faculty of Pharmacy, University of Porto, Rua Aníbal Cunha n°164, 4050-047 Porto, Portugal
[b] Parasite Disease Group, IBMC - Institute for Molecular and Cell Biology, University of Porto, Rua do Campo Alegre, 823, 4150-180 Porto, Portugal
[c] Department of Biological Sciences, Faculty of Pharmacy, University of Porto, Rua Aníbal Cunha n°164, 4050-047 Porto, Portugal
[d] Faculty of Health Sciences, University of Fernando Pessoa, Rua Carlos da Maia, 296, 4200-150 Porto, Portugal
[e] Institute of Biotechnology and Bioengineering, Centre of Genetics and Biotechnology, University of Trás-os-Montes and Alto Douro (IBB/CGB-UTAD), P.O. Box 1013, 5000-801 Vila Real, Portugal

ARTICLE INFO

Article history:
Received 27 January 2012
Received in revised form 15 March 2012
Accepted 16 March 2012
Available online 23 March 2012

Keywords:
Solid lipid nanoparticles (SLN)
Polysorbates
Flow cell cytometry
Fluorescence microscopy
Endocytosis
Human glioma cell lines

ABSTRACT

The aim of this work was to develop a systematic analysis of the cellular internalisation mechanism and pathway of solid lipid nanoparticles (SLN) internalisation. To evaluate if SLN show cell uptake and to understand the mechanism of internalisation, four human glioma cell lines (A172, U251, U373 and U87) and a human macrophage cell line (THP1) were used. For this purpose rhodamine 123 (R123) was loaded into SLN coated with polysorbate 60 and 80. Fluorescence microscopy and flow cell cytometry techniques were assessed to study internalisation of these systems within the cells. MTT studies were performed to evaluate the cytotoxicity of the R123-loaded SLN. To assess the SLN internalisation mechanism and intracellular pathway, excluding endocytosis mechanisms were applied. Our results revealed that R123-loaded SLN with mean size below 200 nm and slight negative surface charge (around −20 mV) have the ability to be internalised by gliomas in a higher amount than by macrophages. The mechanism of internalisation was found to be mainly through a clathrin-dependent endocytic pathway. In addition, the cytotoxicity of SLN was higher for gliomas than for macrophages. These results suggest that SLN can be a promising alternative in brain tumours treatment.

1. Introduction

Malignant gliomas have a very poor prognosis despite the aggressiveness of the current treatment that combines surgery, radiotherapy and chemotherapy (Westphal et al., 2003; Stupp et al., 2006). Knowing that the main obstacle to develop an effective therapy against gliomas is the difficulty of delivering anticancer drugs to the tumour site and cancer cells, several promising drug delivery systems involving nanoparticles were developed (Gelperina et al., 2010; Ying et al., 2010; Cirpanli et al., 2011; Kuo and Liang, 2011).

Solid lipid nanoparticles (SLN) (Joshi and Müller, 2009; Souto and Muller, 2010) have been reported as a promising anticancer drug delivery system to the brain after i.v. injection, due to their ability to cross the blood-brain barrier and deliver drugs to the brain, when coated with proper surfactants, such as polysorbates (Blasi et al., 2007; Brioschi et al., 2007; Kaur et al., 2008; Brioschi et al., 2009). Thus, SLN have high potential in brain tumour treatment.

SLN are colloidal particles, consisting of a matrix composed of lipids being solid at both room and body temperatures, dispersed in an aqueous surfactant solution (Joshi and Müller, 2009). SLN combine advantages of other colloidal drug delivery systems such as emulsions, liposomes and polymeric nanoparticles, and at the same time avoid or minimise some of their drawbacks. Some of the advantages of SLN are the ability to immobilise hydrophilic or hydrophobic drugs in the solid matrix and sustain the drug release, and the ability to prevent the premature degradation of the incorporated drug. Another advantage of the use of lipid particles as drug carrier systems is the fact that the matrix is composed of physiological components and/or excipients of accepted status (FDA-approved constituents), decreasing the risk of acute and chronic toxicity (Joshi and Müller, 2009; Souto and Muller, 2010).

After crossing the blood-brain barrier the next important question is whether the SLN can be internalised by the tumour cell and release anticancer drugs inside them. Nanoparticles located in the external environment of a cell can interact with the plasma membrane, which can lead to the uptake of these nanoparticles

Abbreviations: DAPI, 4',6-diamidino-2-phenylindole, dihydrochloride; PMA, propidium iodide, phorbol 12-myristate 13-acetate; R123, rhodamine 123; SLN, solid lipid nanoparticles.

* Corresponding author. Tel.: +351 222 078 900; fax: +351 222 003 977.
E-mail address: susana.martins@ff.up.pt (S. Martins).

0378-5173/$ – see front matter © 2012 Elsevier B.V. All rights reserved.
doi:10.1016/j.ijpharm.2012.03.032

by the cells through a process named "endocytosis" (Sahay et al., 2010). If the nanoparticles cannot be internalised, the drug can still enter cells after being released from the nanoparticles but the drug can also disperse to the surrounding normal tissues rather than be delivered mainly to the cancer cells. In fact, *in vitro* and *in vivo* studies reveal that the intracellular concentration of the drug is much higher when it is released from nanoparticles into the cytoplasm after internalisation (Sugano et al., 2000; Chen, 2010; Jain et al., 2010).

The form of endocytosis involved in nanoparticles uptake can be expected to affect the nanoparticle's intracellular localisation and trafficking. Understanding endocytic mechanisms is then crucial for the development of nanoparticles for clinical therapies.

Furthermore, most nanoparticles have been shown to exploit more than one pathway to gain cellular entry (Sahay et al., 2010). The endocytosis of nanoparticles also depends on the cell type treated (Lai et al., 2007; Thurn et al., 2007).

Bearing in mind that cell type could be critical in defining the nanoparticle entry and final destination in the cells, we selected four human glioma cell lines (A172, U251, U373 and U87) and one human monocytic cell line (THP1) to study the uptake mechanism of SLN by human glioma cells and macrophages.

Endocytosis is known as a general entry mechanism for various extracellular materials and can be divided into two main categories: phagocytosis (uptake of large particles) and pinocytosis (uptake of fluids and solutes) (Doherty and McMahon, 2009; Sahay et al., 2010). Phagocytosis is followed by specialised professional phagocytes, such as macrophages, monocytes, or dendritic cells. The phagocytic pathway of cellular entry consists of recognising the particles followed by the adhesion of the opsonised particles onto the cell membrane and ingestion of the particle by the cells.

Pinocytosis, in contrast, is present in all types of cells and has multiple forms depending on the cell origin and function. Pinocytosis can be classified as clathrin-mediated endocytosis, caveolae-mediated endocytosis, clathrin- and caveolae-independent endocytosys, and macropinocytosis (Conner and Schmid, 2003).

Internalisation through clathrin-dependent endocytosis happens when the clathrin coat on the plasma membrane develops invaginations in the membrane leading to the budding of clathrin-coated vesicles (Sahay et al., 2010). Nanoparticles localised on the cell membrane could be trapped within the vesicles and brought within the cells. Receptor-mediated endocytosis through clathrin-coated pits is the most common pathway of endocytosis. Alternatively, clathrin-independent endocytosis can happen through the caveolae or lipid-raft pathway. Caveolae are flask-shaped membrane invaginations on cell surfaces that have high amounts of cholesterol and sphingomyelin. Caveolae are abundant in muscle, endothelial cells, fibroblasts and adipocytes and absent in neurons and leukocytes (Conner and Schmid, 2003; Sahay et al., 2010). In the macropinocytosis, the macropinosomes are larger (0.5–10 μm) and distinct from other vesicles formed during pinocytosis. This pathway is possible for virtually any cell with only a few exceptions, such as macrophages and brain microvessel endothelial cells. At first glance, it can internalise large particles with submicron and greater sizes in cells, which lack phagocytosis (Sahay et al., 2010).

To clarify the endocytosis mechanism of nanoparticles internalisation, specific endocytosis mechanisms can be excluded by using pharmacologic inhibitors (Kam et al., 2006; Thurn et al., 2011). Endocytosis is known as a general entry mechanism for various extracellular materials and it is an energy dependent uptake. Consequentially it is inhibited when incubations are carried out at low temperature (e.g. 4 °C instead of 37 °C) (Kam et al., 2006; Thurn et al., 2011). Furthermore, to assess the role of clathrin in the internalisation of SLN, incubations under hypertonic environments (e.g. sucrose 0.45 M) that are recognised to disrupt the formation of clathrin-coated vesicles on the cell membrane could be carried out (Kam et al., 2006; Sahay et al., 2010). To evaluate SLN cellular uptake through the caveolae or lipid-rafts pathway, cells could be pretreated with the drug filipin, which is known to disrupt the cholesterol distribution within the cell membrane (Kam et al., 2006; Sahay et al., 2010). To assess if the cellular entry occurs by macropinocytosis (gliomas) or phagocytosis (macrophages) the cells could be pretreated with cytochalasin B, a potent inhibitor of macropinocytosis/phagocytosis, which depolymerises the actin filaments avoiding the formation of the structures essential to enclose particulates (Serda et al., 2009).

The cells with excluded endocytosis mechanisms were studied along with the 5 cell lines by flow cell cytometry allowing determination of the uptake pathway of the SLN. Furthermore, fluorescence microscopy was performed to visualise SLN uptake and distribution within the cells.

The aim of this work was to develop a systematic analysis of the cellular internalisation mechanism and pathway for SLN to understand the mechanisms behind this internalisation.

2. Materials and methods

2.1. Materials

The wax cetyl palmitate was a gift from Gattefossé SA (France). The surfactants polysorbate 60 and 80 were provided by Merck (KgaA, Germany). Rhodamine 123 (R123), thiazolyl blue tetrazolium bromide (MTT assay), propidium iodide, phorbol 12-myristate 13-acetate (PMA), collagen from rat tail, filipin III from *Streptomyces filipinensis* (Filipin) and cytochalasin B were obtained from Sigma–Aldrich (Portugal). 4',6-diamidino-2-phenylindole, dihydrochloride (DAPI) and Alexa Fluor® 594 conjugated of wheat germ agglutinin (Alexa) were obtained from Molecular probes (USA). D(+)-Sucrose was purchased from Romil Pure Chemistry (UK). Dulbecco's Modified Eagle's Medium (DMEM), fetal bovine serum (FBS), glutamine, penicillin-streptomycin, Fungizone, RPMI Medium 1640 and Hanks' balanced salt solution (HBSS) were provided by Gibco (Invitrogen Corporation, Spain). Dimethyl sulfoxide (DMSO) was obtained from Merck (KgaA, Germany). Purified water was of MilliQ®-quality.

2.2. Annotation for formulation

Unique codes were selected for identifying the produced formulations; it consists of abbreviations for the fluorescent probe R123; the lipid cetyl palmitate (CP) and the surfactants polysorbate 60 (P60) and polysorbate 80 (P80). CP60 and CP80 stand for unloaded cetyl palmitate-based SLN stabilised with polysorbate 60 or polysorbate 80; respectively. R123-CP60 and R123-CP80 stand for rhodamine 123 incorporated into cetyl palmitate-based SLN stabilised with polysorbate 60 or polysorbate 80; respectively.

2.3. Methods

2.3.1. Production of solid lipid nanoparticles

Formulations containing the lipid cetyl palmitate and the surfactants polysorbate 60 or 80, were prepared at concentrations of 5% (w/w) of lipid and 2% (w/w) of surfactant. One lipid and one surfactant were combined at a time. SLN were prepared by the high shear homogenisation and ultrasonication techniques. Briefly, the lipid and surfactant mixture was melted at approximately 5–10 °C above the melting point of the lipid. Water was heated at approximately the same temperature and transferred to the surfactant

lipid mixture. A pre-emulsion consisting of lipid and of surfactant in water were prepared with an ultra-turrax T25 (IKA-Labortechnik, Germany) at 8000 rpm for 30 s, and an ultrasonication probe at 70% amplitude for 2.5 min (VibraCell model VCX 130 equipped with a 6 mm probe, Sonics & Materials, Inc., Newtown, CT, USA). R123-loaded SLN were prepared by adding the fluorescent dye (0.04% w/w) to the molten lipid prior to particle preparation. SLN were washed with water (~1:2 v/v) using centrifugal filter units (Amicon Ultra, Ultra cell-50K), (Milipore, Carrigtwohill, Co. Cork, Ireland) until no R123 was detected in the supernatant. R123 detection was performed using the UV spectrophotometer (Jasko V-650 Spectrophotometer, Japan). Generally, after washing the SLN 3–4 times no R123 was detected in the supernatant.

2.3.2. Assessment of particle size and size distribution

Particle size and distribution (polydispersity index) was determined by dynamic light scattering (DLS), using a Zetasizer Nano ZS laser scattering device (Malvern Instruments Ltd., Malvern, UK). The samples were diluted with water with a conductivity adjusted to 50 μS/cm and analysed; the available software (Zetasizer Nano Series V6.20) was used to correlate the intensity of scattered light (at a backscattering angle of 173°) with the hydrodynamic radius of the spherical particle. Several dilutions of the sample were tested at 25 °C to obtain dispersed and isolated nanoparticles in the solvent. The particle size determination allows monitoring the nanoparticles preparation method and verifying its time dependent stability regarding the tendency for aggregation and sedimentation. For each sample, the mean diameter ± standard deviation of at least three determinations was calculated applying multimodal analysis. SLN stability was assessed by measuring the mean particle diameter and polydispersity index of SLN immediately after production and after storage at 4 °C, room temperature and 40 °C during two months. SLN stability in culture medium was also assessed by measuring the mean particle diameter and polydispersity index of SLN diluted in complete culture medium during 3 and 15 days.

2.3.3. Zeta potential

The electrophoretic mobility (zeta potential) of the nanoparticles and ultimately their surface charge was measured by combining laser Doppler velocimetry and phase analysis light scattering (PALS) using a Zetasizer Nano ZS (Malvern, Worcestershire, UK). The samples, diluted with water with a conductivity adjusted to 50 μS/cm by dropwise addition of 0.9% (m/v) NaCl solution, were placed in polystyrene cuvettes with platinum electrodes and then applied an electric field across the dispersion of the nanoparticles. Surface charged particles within the dispersion migrated toward the electrode of opposite charge and the velocity of particles migration was converted in zeta potential values by using the Smoluchowski's equation. The zeta potential results reported are the mean ± standard deviation of at least three determinations.

2.3.4. Differential scanning calorimetry analysis

The study of the physical state and polymorphism of the SLN was performed by differential scanning calorimetry (DSC) using a DSC 200 F3 Maia (Netzsh–Gerätebau GmbH) and Proteus Analysis software. The samples were weighed (5–10 mg) directly in aluminium pans and scanned between 25 °C and 85 °C at a heating and cooling rate of 5 °C/min under nitrogen gas. DSC analyses were performed on bulk lipids and SLN on the day of production. The degree of crystallinity or recrystallisation index (RI) was determined by the following equation:

$$\mathrm{RI}[\%] = \frac{\text{Enthalpy SLN}[\mathrm{J/g}]}{\text{Enthalpy bulk material}[\mathrm{J/g}] \times \text{Concentration lipid phase}[\%]} \times 100$$

2.3.5. Cell culture

The human glioma A172, U251, U373 and U87 cell lines (ATCC) were maintained in complete Dulbecco's Modified Eagle's Medium (DMEM, Gibco, Invitrogen Corporation) supplemented with 10% FBS, 1% glutamine (2 mM) and 1% antibiotic-antimycotic (Gibco, Invitrogen Corporation: 10,000 units/mL penicillin G sodium, 10,000 mg/mL streptomycin sulphate and 25 mg/mL amphotericin B as Fungizone) in a humidified incubator (Heraeus Hera Cell incubator) at 37 °C under 5% CO_2 atmosphere. Cells were subcultured every 3–5 days using trypsin.

The human monocytic THP1 cell line (Health Protection Agency, UK) was cultured in suspension in RPMI-1640 complete growth medium supplemented with 10% FBS, 1% glutamine (2 mM) and 1% antibiotic-antimycotic (Gibco, Invitrogen Corporation): 10,000 units/mL penicillin G sodium and 10,000 mg/mL streptomycin sulphate, in a humidified incubator (Heraeus Hera Cell incubator) at 37 °C under 5% CO_2 atmosphere. These cells were differentiated into macrophage phenotype by resuspension in THP1 medium, supplemented with 100 ng/mL PMA seeded at a density of 1×10^6 cells per well or cover-slip, previously treated during at least 4 h with an aqueous solution of collagen I (24 μg/mL), for 18 h. After that period, cells were washed with HBSS and let 24 h at 37 °C in RPMI 1640 medium before experiments. THP1 differentiated macrophages adhered to the surface of the cover-slips and wells.

2.3.6. Fluorescence microscopy

Uptake studies of fluorescent SLN by cells were carried out by fluorescence microscopy. R123 was used as a fluorescence probe to investigate the cellular uptake of R123-loaded SLN. Unencapsulated R123 was removed by filtration using centrifugal filter devices (Amicon® Ultra, Ultra cell-50k, Millipore, USA). The experiment was conducted in a six-well culture plate. Cell numbers were adjusted in order to get 1×10^5 cells in each well on sterile glass coverslips (22 mm × 22 mm) previously treated with collagen I. Cells were incubated at 37 °C, 5% CO_2 until their adherence on glass cover-slips (overnight) in supplemented DMEM medium. Then, adherent cells were treated with 1 mL of 500 μg/mL of R123-loaded SLN (1.4 μg/mL R123) diluted in DMEM medium, during an incubation period of 2 h. The cells were washed three times with HBSS, and then stained with 1 mL of Alexa Fluor®594 (cellular membrane stain; excitation/emission maxima ~590/617 nm) solution 1 μg/mL diluted in HBSS for 10 min at 37 °C, and with 1 mL of DAPI (nuclear stain; excitation/emission maxima ~358/461 nm) solution 300 nM during the same time. After each staining procedure, cells were washed three times with HBSS. Finally, cells were fixed in cold methanol (−20 °C) and after that imaged with a fluorescence microscope. Cellular imaging was captured under a Nikon Eclipse E400 fluorescence microscope (400× magnification) equipped with digital camera and processed using Nikon ACT-2U® software. Selected wavelengths were 365–375 nm (DAPI, blue), 450–490 nm (R123, green) and 510–560 nm (Alexa Fluor® 594, red).

All the experimental steps were performed considering light protection with aluminium sheet to avoid fluorescent dequenching.

2.3.7. MTT assay

Cell viability following exposure to an uptake of SLN was measured by using the MTT assay (Mosmann, 1983) with some adjustments. 200 μL of cell suspension with 1×10^5 cells per mL were seeded into wells of 96-well tissue culture test plates (Orange Scientific products, Belgium). The samples of SLN (concentrations from 50 μg/mL to 5000 μg/mL of solid amount) were added and incubated for 24 h at 37 °C in 5% CO_2. The medium with the SLN was removed and MTT solution (5 mg/mL MTT in supplemented DMEM medium) was added to the cultures (final concentration of 0.5 mg/mL) and incubated for 4 h at 37 °C. The medium with

Table 1
Uptake pathways and inhibition conditions.

Pathway	Inhibitor	Mechanism	References
Endocytosis	4 °C	Blocks energy dependent process	Kam et al. (2006), Thurn et al. (2011)
Clathrin-mediated endocytosis	Sucrose (0.45 M)	Inhibits clathrin-mediated endocytosis	Sahay et al. (2010), Kam et al. (2006)
Caveolae-mediated endocytosis	Filipin (5 μg/mL)	Inhibits caveolae-mediated endocytosis	Sahay et al. (2010), Kam et al. (2006)
Phagocytosis	CytB (5 μg/mL)	Depolymerises the actin filaments avoiding the formation	Serda et al. (2009)
Macropinocytosis	CytB (5 μg/mL)	of the structures essential to enclose particulates	Serda et al. (2009)

MTT solution was discarded and formazan crystals were solubilised using 150 μL DMSO. Subsequently, an incubation of 15 min under light protection and at room temperature was performed. Absorbance which is directly proportional to cellular metabolism was measured at 550 nm and 690 nm (background subtraction) in a Power Wavex microplate spectrophotometer (BioTek Instruments Inc., USA). Cell viability was expressed in percentage compared to untreated cells.

2.3.8. Flow cell cytometry

SLN uptake by the cell lines were further investigated using flow cell cytometry (Becton Dickinson FACSCalibur, USA). For that 1 mL of cell suspension with 1×10^6 cells per mL being seeded 24 h before the experiments into wells of 24-well tissue culture test plates (Orange Scientific products, Belgium). For A172, U87 and THP1 cell lines the wells were previously treated with collagen I (rat tail) to increase the adhesion of these cells to the wells. The samples of R123-loaded SLN at 50 μg/mL of solid content (0.14 μg/mL R123) were added and incubated for 2 h at 37 °C in 5% CO_2. After incubation, the cells were washed three times with HBSS. Adherent cells were detached from the surface by treatment with trypsin and resuspended in ice-cold HBSS. Propidium iodide was added to the cells at a final concentration of 0.2% and immediately analysed with a FACS Calibur using a 488 nm laser for excitation of R123 and a band centred at 530 nm for detection of fluorescence. Flow cytometry data were processed to remove the events associated to free nanoparticles according to their light scattering properties. From the filtered data, the arithmetic mean of the fluorescence intensity of cells exposed to the various formulations was determined, and the data was analysed using FlowJo software. Cells that were stained with propidium iodide (corresponding to naturally occurring dead cells) were excluded from the data analysis.

Table 1 depicts endocytosis inhibitors selected for this work, their pathway and mechanism of endocytosis inhibition.

Analysis of endocytosis mechanism was similar to that previously described, however, for this case the cells were exposed to several endocytosis inhibitors (4 °C, sucrose 0.45 M, filipin and cytochalasin B) 30 min before the exposition of the cells to the R123-loaded SLN and during all the exposition. For assessing if the endocytosis is the main entry of the SLN into the cell, endocytosis was inhibited by incubating the cells at 4 °C instead the regular 37 °C condition. Clathrin dependent endocytosis was inhibited exposing the cells to 0.45 M sucrose 30 min before and during exposure to the R123-loaded SLN at 37 °C. For caveolae-mediated endocytosis inhibition cells were pretreated in medium supplemented with filipin (5 μg/mL) for 30 min followed by exposure to the R123-loaded SLN at 37 °C.

For macropinocytosis/phagocytosis inhibition cells were pretreated in the medium supplemented with cytochalasin B (5 μg/mL) for 30 min followed by exposure to the R123-loaded SLN at 37 °C.

2.3.9. Statistical analysis

For the SLN physicochemical characterisation results are shown as the mean ± standard deviation (SD) of at least 3 different batches of the same formulation. The *t*-test and the one-way analysis of variance (ANOVA) were performed to compare two or multiple groups, respectively. If the group in each time interaction was significantly different ($P < 0.05$), differences between groups were compared within a post hoc test (Tukey HSD). To describe statistical differences with controls, the Dunnett test was used. Results are reported as a mean ± SD from a minimum of three independent experiments performed in cells pertaining to different passages. Differences were considered significant at $P < 0.05$. All statistical analyses were performed with the software PASW Statistic 18 (SPSS Inc., Chicago, USA).

3. Results

3.1. Physicochemical characterisation of solid lipid nanoparticles

Unloaded SLN were produced and characterised in terms of mean diameter, polydispersity index and zeta potential for two months to assess the stability of these systems during storage. SLN with a mean diameter between ~130 and 165 nm, low polydispersity index <0.3 and with slight zeta potential values between −18 and −23 mV have been produced and were stable in terms of mean diameter for at least two months at the three temperatures tested (4 °C, 22 °C and 40 °C). SLN stabilised with polysorbate 60 showed a slightly smaller mean diameter and a higher stability than SLN stabilised with polysorbate 80 (Fig. 1).

R123 was then incorporated into SLN stabilised by polysorbate 60 (R123-CP60) or 80 (R123-CP80) as a model drug and a fluorescent dye. Analysis of the R123-loaded SLN revealed just a slight increase in the mean diameter of the SLN indicating no influence of the R123 incorporation in the physicochemical characteristics of these systems (Table 2). For analysing the stability of the SLN during the *in vitro* experiments in cells, the four formulations (CP60, R123-CP60, CP80 and R123-CP80) were incubated in the culture medium for two weeks. The obtained results revealed only a small increase in the mean diameter of the SLN in the culture medium indicating no formation of agglomerates or aggregates that could interfere with the *in vitro* experiments.

Thermal behaviour of cetyl palmitate bulk and cetyl palmitate-based SLN was assessed by DSC. The DSC results obtained are depicted in Fig. 2 and Table 3. When the bulk was heated from 25 °C to 85 °C, a number of thermal transitions were observed (Fig. 2A). Two endothermic peaks were observed at around 47 °C (small shoulder) and 57 °C corresponding to the melting of α and β polymorphic forms of crystal lipids, respectively. The same number of thermal transitions was detected with the samples of formulations stored at 4 °C, 22 °C and 40 °C. However, the onset temperature and the melting peak of the SLN were approximately 4–7 °C lower than those obtained for the bulk materials (Fig. 2 and Table 3).

The DSC scans of all the cetyl palmitate-based SLN shows that independently of the surfactant used as stabiliser (polysorbate 60 or 80) the α and β modifications are observed at the same temperature, however the evidence and area of the peaks are different.

DSC is also useful to evaluate the degree of crystallinity of lipid materials. The degree of crystallinity of pure lipids and SLN was estimated by comparison of the melting enthalpy of the bulk material with the melting enthalpy of the dispersion. The

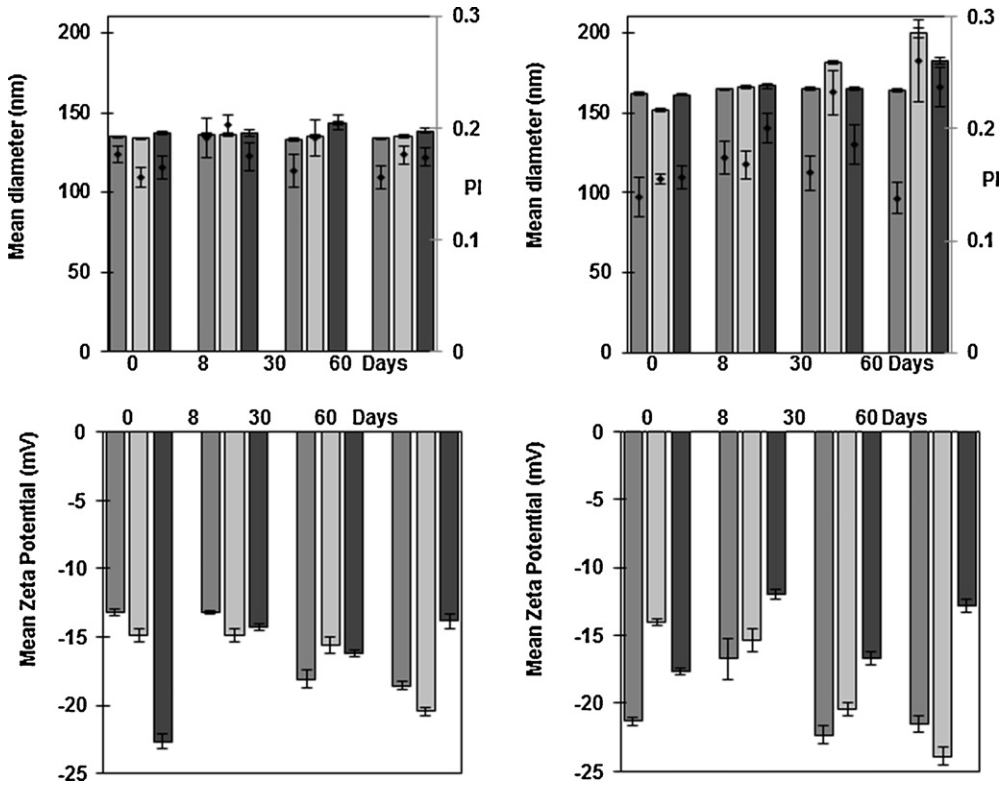

Fig. 1. Physicochemical characteristics of cetyl palmitate-based solid lipid nanoparticles (SLN) stabilised with polysorbate 60 (CP60) and 80 (CP80). Mean diameter, polydispersity index (PI)(up) and zeta potential (down) (mean ± SD) of the SLN CP60 (left) and CP80 (right) stored at 4 °C (■), 22 °C(■) and 40 °C(■), determined on the day of production and after 8, 30 and 60 days of storage.

Table 2
Physicochemical characteristics of solid lipid nanoparticles (SLN). Mean size, polydispersity index (PI) and zeta potential (ZP) of SLN on day production and dispersed in culture medium.

Sample	Mean size ± SD (nm)	PI ± SD	ZP ± SD (mV)
CP60	134.70 ± 7.55	0.195 ± 0.02	−17.96 ± 1.3
CP60 in DMEM 3 days	147.92 ± 6.77	0.193 ± 0.01	
CP60 in DMEM 15 days	158.25 ± 7.71	0.250 ± 0.02	
R123-CP60	157.20 ± 7.56	0.212 ± 0.01	−22.75 ± 1.5
R123-CP60 in DMEM 3 days	162.67 ± 6.72	0.250 ± 0.02	
CP80	148.70 ± 7.92	0.208 ± 0.04	−18.77 ± 2.4
CP80 in DMEM 3 days	165.09 ± 6.83	0.205 ± 0.02	
CP80 in DMEM 15 days	174.01 ± 8.54	0.201 ± 0.01	
R123-CP80	165.32 ± 8.26	0.265 ± 0.01	−20.55 ± 1.5
R123-CP80 in DMEM 3 days	174.15 ± 6.99	0.284 ± 0.01	

values were extracted by DSC scans using appropriate software. DSC analysis revealed that the SLN are in the desired solid state and that the degree of crystallinity of the investigated SLN was found to be between 53 and 73% (Table 3).

3.2. In vitro studies in cells

R123-loaded SLN emit detectable fluorescence that can be analysed by both fluorescence microscopy and flow cytometry. SLN were stable in terms of mean diameter in culture medium for at

Table 3
DSC parameters of solid lipid nanoparticles (SLN). Onset and melting temperatures, melting enthalpies and recrystallisation index (RI) of cetyl palmitate-based SLN stabilised with polysorbate 60 (CP60) and 80 (CP80) stored at 4 °C, 22 °C and 40 °C.

Sample	Storage temp (°C)	Onset (°C)	Enthalpy ΔH (J/g)	Melting point (°C)	RI (%)
CP80	4	48.9	7.97	50.5	60
	22	49.2	9.23	51.0	69
	40	48.9	7.05	50.6	53
CP60	4	46.4	9.66	49.8	73
	22	48.3	9.22	50.2	69
	40	48.9	7.97	50.5	60
CP bulk	22	53.2	266.5	57.0	100

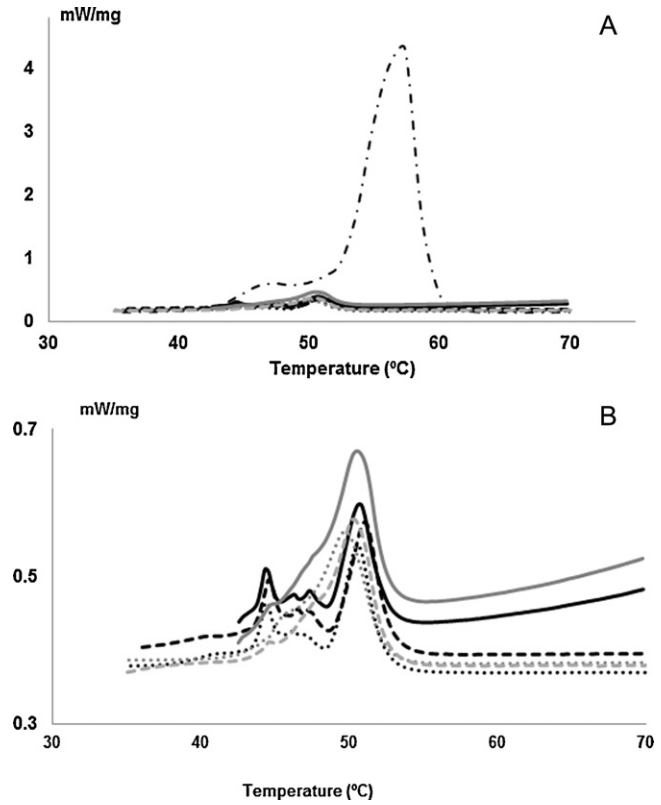

Fig. 2. DSC thermograms of the bulk cetyl palmitate (CP), solid lipid nanoparticles (SLN) stabilised with polysorbate 60 (CP60) and 80 (CP80). (A) DSC thermograms of the bulk CP (-. -) and the SLN CP80 (black) and CP60 (grey) stored at 4 °C (..), 22 °C (- -), and 40 °C (_). (B) DSC thermograms of CP80 (black) and CP60 (grey) stored at 4 °C (..), 22 °C (- -) and 40 °C (_).

least two weeks. The experiments described herein characterise the uptake of R123-loaded SLN by A172, U251, U373, U87 and THP1 human cells.

3.2.1. *Relative uptake of solid lipid nanoparticles in human cell lines*

In order to confirm the uptake of SLN by the cells in study, cells were incubated during 2 h with R123-loaded SLN (R123-CP60 and R123-CP80) and were analysed by fluorescence microscopy (Fig. 3).

Since R123 was not covalently bound to the SLN, we cannot exclude the possibility that R123 might be released from the SLN during cell uptake. To eliminate any interference, cells were incubated with free R123, unloaded SLN and R123-loaded SLN, separately under same experimental conditions. After 2 h of incubation, cells were processed and viewed under fluorescence microscope. Cells cultured with only free R123 and unloaded SLN showed negligible fluorescence outside and inside the cells, while an intense green fluorescence was seen inside the cells cultured with R123-loaded SLN. The unloaded SLN and the free R123 were used as a negative control to confirm that the lipid matrix does not show native fluorescence that potentially could interfere with R123 and that if the free R123 is released from the nanoparticles during the experiment it will not interfere with it.

R123-loaded SLN have green fluorescence, while the cell membranes appear in red, since it was stained with Alexa Fluor® 594 and the nucleus appear in blue, since it was stained with DAPI. After 2 h of incubation a strong green fluorescence was observed inside all the cells (Fig. 3), corresponding to a large number of R123-loaded SLN that were internalised.

3.2.2. *Effect of solid lipid nanoparticles on cell viability and cytotoxicity*

To address cell viability and cytotoxicity the MTT assay was performed, the cells being incubated with freshly prepared nanoparticles for 24 h.

The viability of the cells after 2 h of exposition to R123-SLN and to the excluded endocytosis conditions (4 °C, sucrose 0.45 M, filipin and cytochalasin B) were verified by a parallel study using propidium iodide incorporation evaluated by flow-cytometry and revealed no toxicity (viability higher than 90%) for all cell lines (data not shown). Subsequently, at the experimental internalisation conditions, the formulations revealed no significant toxicity for all cell lines.

Uptake of nanoparticles (24 h incubation) did not disturb A172 and THP1 normal cell propagation and showed more than 90% cell viability, when cells were incubated with 50 μg/mL of solid amount of R123-loaded SLN, relative to control cells (medium) (Fig. 4). For U251, U373 and U87 viability was significantly reduced when cells were incubated with 50 μg/mL and at 500 μg/mL of solid amount of R123-loaded SLN, viability was reduced to 45–66% (Fig. 4). These results suggest that SLN was internalised more by glioma cell lines and show more cytotoxicity against these cells (except A172) than to macrophages

Analysing Fig. 5, it is evident that SLN at higher concentrations are more cytotoxic against glioma cells than to macrophages.

3.2.3. *Uptake mechanism of solid lipid nanoparticles*

A systematic analysis of the cellular internalisation mechanism and pathway was followed of R123-loaded SLN. Since cells do not exhibit significant fluorescence on their own as confirmed by flow cytometry (Figs. 6 and 7), it is assumed that the fluorescence levels measured in cells are due to R123-SLN uptake.

Fig. 6 presents histograms of flow cytometry assays in cells after 2 h incubation with, SLN stabilised with polysorbate 60 (R123-CP60, —), or stabilised with polysorbate 80 (R123-CP80, ---). No significant differences could be detected between the two formulations in terms of FL1 values, indicating similar amount of fluorescent cells counted and therefore similar internalisations.

Fig. 7 shows the mean fluorescence of the cells after 2 h of incubation with R123-loaded SLN and reveals that for all the cells there is always significant internalisation of the R123-loaded SLN. Furthermore, the internalisation is significantly higher in the gliomas A172 and U87 than in the macrophages (THP1), being the mean fluorescence higher more than twice. These results indicate that SLN are more easily and rapidly internalised in glioma than in macrophages cell lines.

Again, no significant differences could be observed between the two SLN formulations in terms of mean fluorescence values indicating similar internalisations of both formulations.

Generally, there are two modes of entry, either R123-loaded SLN transverse the cell membrane via endocytosis or energy independent non-endocytotic mechanism. However, the endocytosis could be sub-categorised in phagocytosis and pinocytosis (clathrin-mediated endocytosis, caveolae-mediated endocytosis, clathrin- and caveolae-independent endocytosis, and macropinocytosis) pathways (Fig. 8).

To clarify the mechanism of internalisation behind the R123-loaded SLN internalisation a series of investigations on uptake mechanism and cellular internalisation were carried out for R123-loaded SLN with the cells exposed to specific endocytic inhibitors (Table 1). To better compare the obtained data, the SLN uptake values were expressed as relative fluorescence, which is the total fluorescence in the cells after incubation in presence of inhibitors with the R123-loaded SLN samples calculated as relative percentage of the positive control (fluorescence of the cells incubated under normal conditions (2 h at 37 °C) assumed 100%.

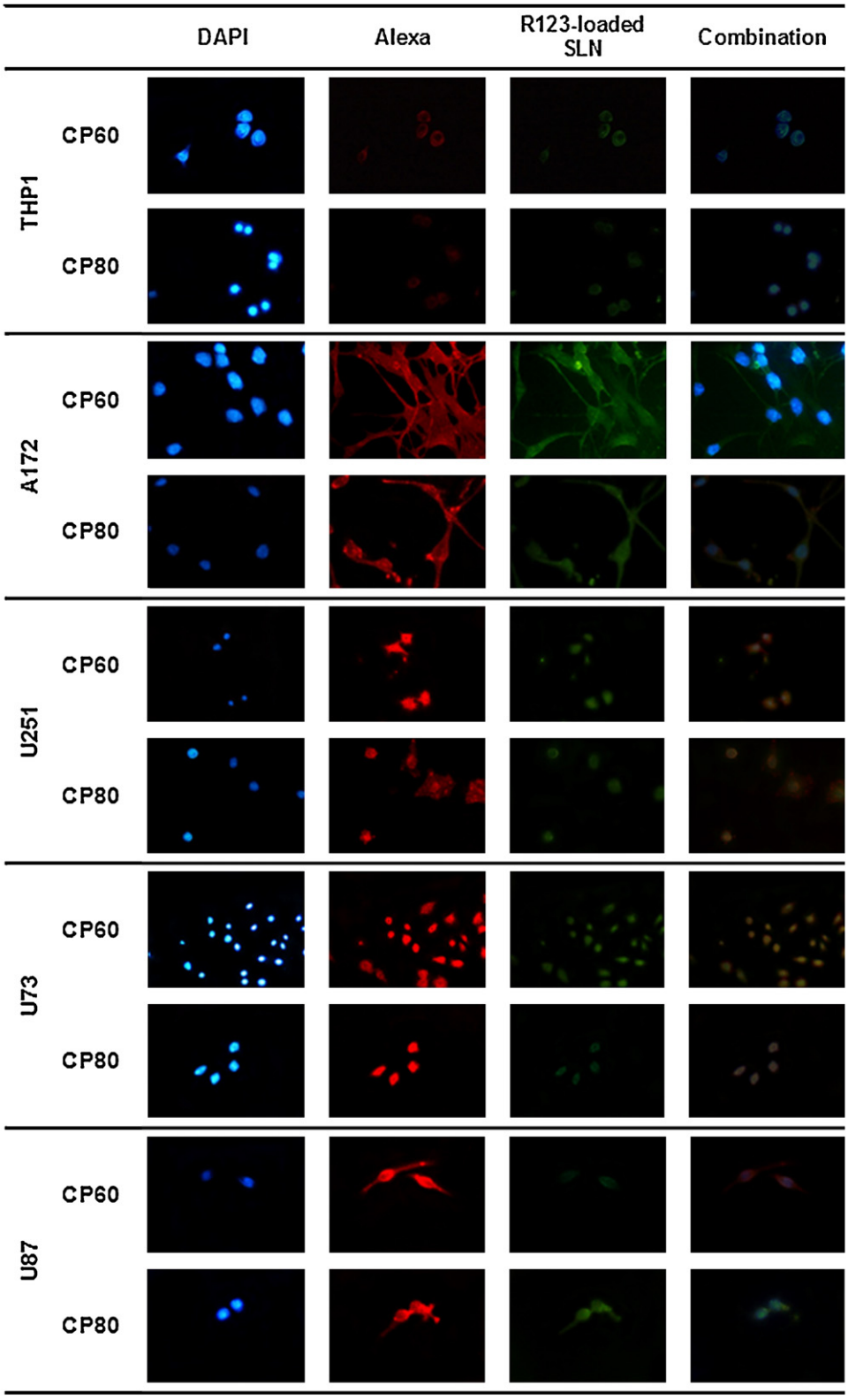

Fig. 3. Rhodamine 123 (R123)-loaded solid lipid nanoparticles (SLN) cell uptake. Fluorescence microscope images of R123-loaded SLN uptake (2 h) by THP1, A172, U251, U373 and U87 cell lines. Nucleus are stained with DAPI (blue) and cell membrane with Alexa (red). R123-loaded SLN shown green fluorescence. Representative images are shown. (Magnification 400×).(For interpretation of the references to colour in this figure legend, the reader is referred to the web version of the article).

Endocytosis is an energy dependent mechanism. The process is hindered at a low temperature (at 4 °C instead of 37 °C). Cellular incubations with R123-loaded SLN were carried out at 4 °C in parallel with the regular (37 °C) incubation conditions, thereby hampering the endocytosis process. In fact, the level of fluorescent intensity inside each cultured cell was reduced drastically (statistically significant) relative to cells cultured in regular standard conditions (Fig. 9).

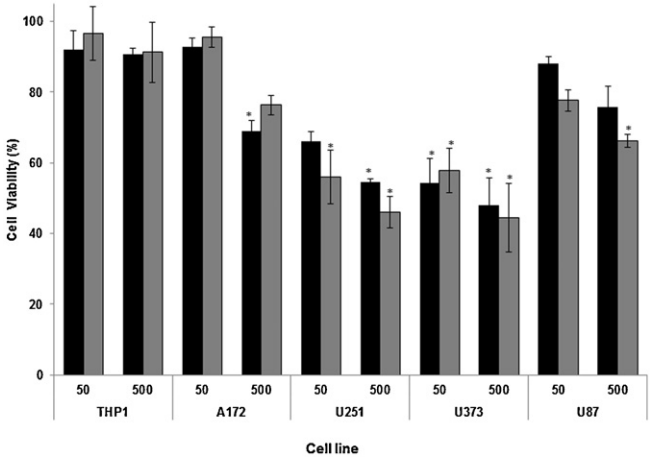

Fig. 4. Cell viability (mean ± SD) of the cells exposed at rhodamine 123 (R123)-loaded solid lipid nanoparticles (SLN) stabilised with polysorbate 60 (R123-CP60) and 80 (R123-CP80). Viability of different cells (THP1, A127, U251, U373 and U87) exposed for 24 h at R123-CP60 and R123-CP80 at the concentrations of 50 and 500 μg/mL of solid content.

This reduction therefore indicates endocytosis as the internalisation mechanism for the uptake of R123-loaded SLN at 37 °C.

To evaluate the contribution of each of the three main energy-dependent pathways of non-phagocytic endocytosis on the internalisation of R123-loaded SLN, each mechanism was inhibited in turn.

To assess the role of clathrin in the internalisation of R123-loaded SLN, we carried out incubations under conditions that are known to disrupt the formation of clathrin-coated vesicles on the cell membrane. This treatment consisted of pretreating the cells with 0.45 M of sucrose (hypertonic treatment) medium prior to exposure to the R123-loaded SLN. These pretreatments drastically reduced the level of cellular uptake of R123-loaded SLN as deduced from the cell cytometry data (Fig. 10A), therefore suggesting the clathrin pathway for endocytotic cellular uptake of R123-loaded SLN.

To further elucidate R123-loaded SLN cellular uptake, we investigated the possibility of cellular entry by R123-loaded SLN via caveolae or lipid raft pathway. As caveolae dependent cell entry relies on the presence of cholesterol domains, we pretreated cells with the drug filipin which disrupts the cholesterol distribution within the cell membrane. Fig. 10B shows the flow cytometry data obtained after incubations in R123-loaded SLN for cells with and without filipin pretreatment, respectively. In stark contrast to the clathrin-blocking experiments, we observed that pretreatment of cells with filipin had no blocking effect on the cellular uptake of R123-loaded SLN, which suggests little or no involvement of the caveolae-dependent cell-entry pathway for R123-loaded SLN. In addition, for the THP1 and A172 cell lines the uptake of R123-loaded SLN was increased when exposed to filipin. Similar results were obtained by Tahara et al. (Tahara et al., 2010) when in A549 cells were pretreated with filipin.

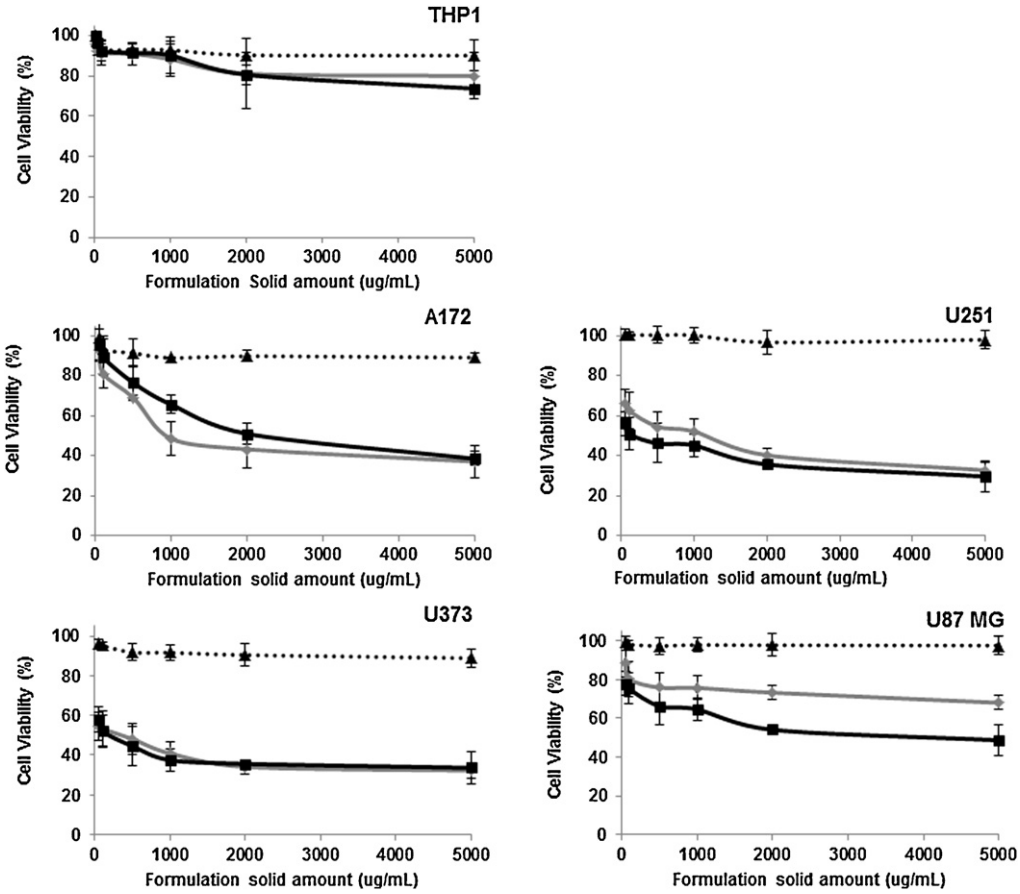

Fig. 5. Cell viability (mean ± SD) of different cells after incubation with cetyl palmitate-based solid lipid nanoparticles (SLN) stabilised with polysorbate 60 (CP60) and 80 (CP80). Cell viability of THP1, A172, U251, U373 and U87 incubated for 24 h with CP60 (♦), CP80 (■) and water (▲).

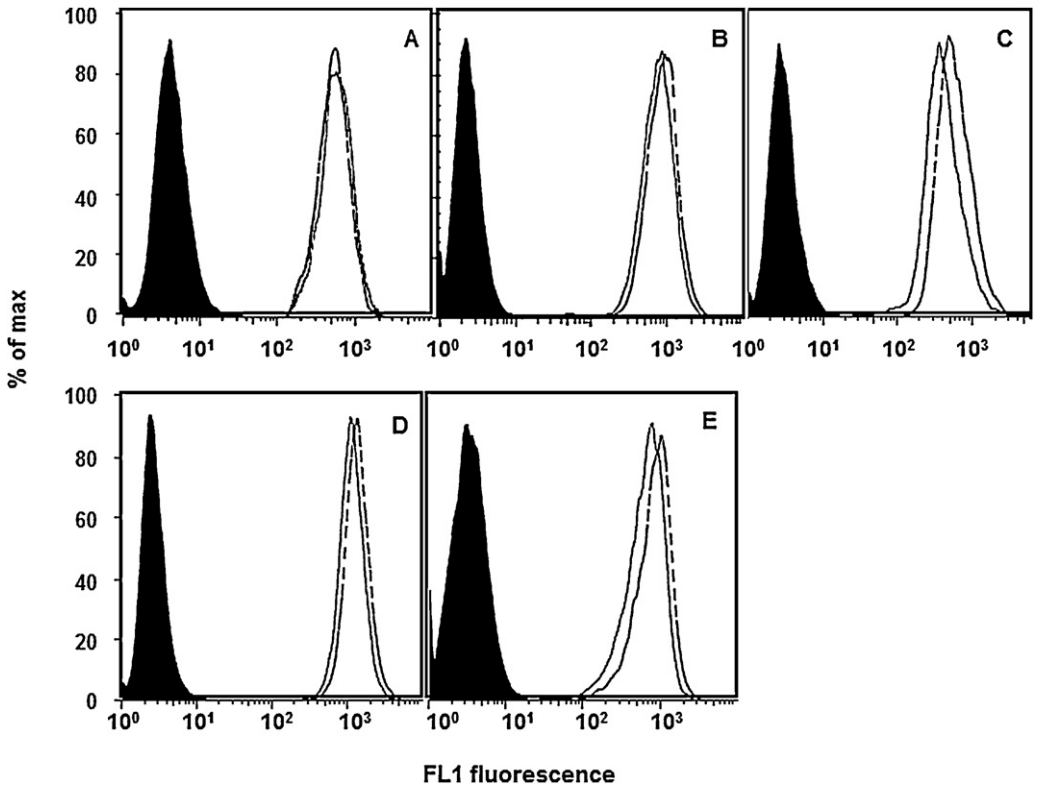

Fig. 6. Uptake of rhodamine 123 (R123)-loaded solid lipid nanoparticles (SLN) stabilised with polysorbate 60 (R123-CP60) and 80 (R123-CP80). Flow cytometry histograms data for THP1 (A), A172 (B), U251 (C), U373 (D) and U87 (E) in medium (control (black)) and that were incubated with R123-CP60 (—) or R123-CP80 (⁻).

Taken together, our experimental data suggest that cellular internalisation of R123-loaded SLN is through the clathrin-dependent endocytosis pathway.

To assess the involvement of macropinocytosis/phagocytosis in R123-loaded SLN uptake, cells were preincubated with cytochalasin B, which is known to depolymerise the actin filaments which are necessary to the formation of the structures essential to enclose particulates. Fig. 11 reveals that a significant reduction of the internalisation of the R123-CP80 occurred in the A172 and U87 cell lines. However, this inhibition was much smaller than that resulting from the exposition to the hypertonic environment. These results indicate that for some cells more than one mechanism could

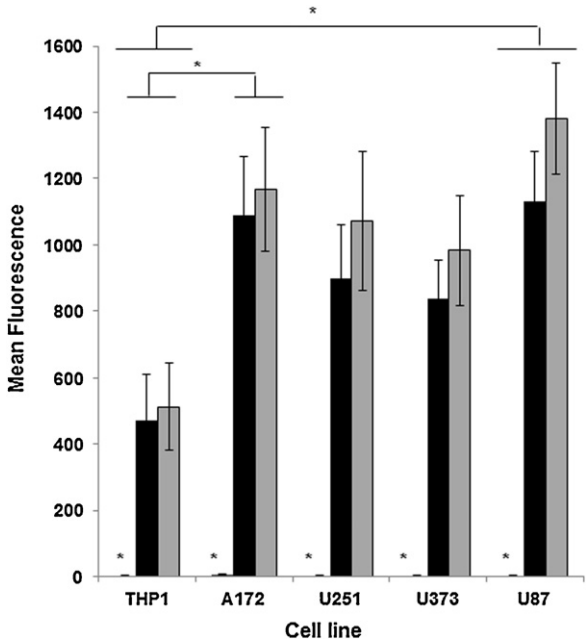

Fig. 7. Uptake mean (fluorescence mean ± SD) of rhodamine 123 (R123)-loaded solid lipid nanoparticles (SLN) stabilised with polysorbate 60 (R123-CP60) and 80 (R123-CP80). Flow cytometry data for THP1, A172, U251, U373 and U87 in medium (control (■)) and that were incubated with R123-CP60 (■) or R123-CP80 (■). Control (cells) was always significant different than cells incubated with R123-loaded SLN.

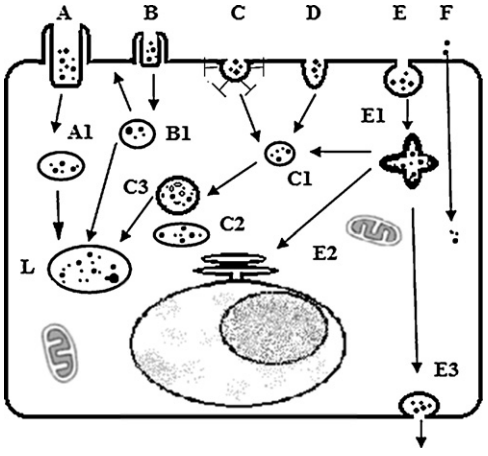

Fig. 8. Cellular internalisation of nanoparticles and associated intracellular trafficking. (A) Phagocytosis, leading to phagosomes (A1) and phago-lysosomes (L). (B) Macropinocytosis, engulfing nanoparticles, forming macropinosomes (B1) which can be exocytosed or fused with lysosomes (L). (C) Clathrin-mediated endocytosis, leading to primary endosomes (C1) and late endosomes (C2) with multivesicular bodies (C3). (D) Clathrin- and caveolae-independent endocytotic pathways. (E) Caveolae-mediated endocytosis, leading to caveosomes (E1) which fuse with the endoplasmic reticulum (E2) or translocate through the cell (E3). (F) Particle diffusion or transport through the apical plasma membrane, leading to particles situated in the cytosol. Figure and descriptions are adapted from Brandenberger et al. (2010), Hillaireau and Couvreur (2009).

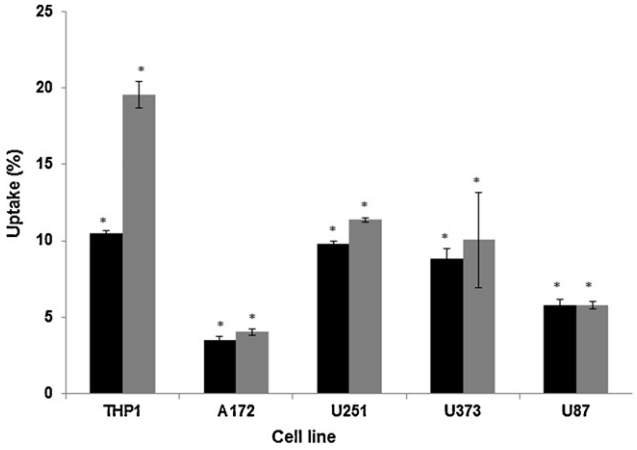

Fig. 9. Effect of temperature on rhodamine 123 (R123)-loaded solid lipid nanoparticles (SLN) internalisation (fluorescence mean ± SD). Cells were treated with 50 μg/mL of R123-loaded SLN stabilised with polysorbate 60 (R123-CP60, ■) and 80 (R123-CP80, ■) at 4 °C. Subsequent analysis by flow cytometry showed a significant decrease in fluorescence for all cells treated at 4 °C compared with 37 °C (100% uptake).

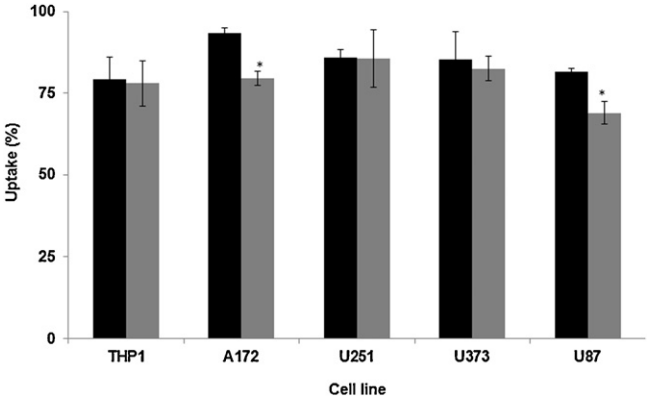

Fig. 11. Effect of macropinocytosis/phagocytosis inhibition on rhodamine 123 (R123)-loaded solid lipid nanoparticles (SLN) internalisation (fluorescence mean ± SD). Cells were pretreated with cytochalasin B (5 μg/mL) during 30 min and then treated with 50 μg/mL of R123-loaded SLN stabilised with polysorbate 60 (R123-CP60, ■) and 80 (R123-CP80, ■). Subsequent analysis by flow cytometry showed a significant decrease in fluorescence only for A172 and U87 incubated with R123-CP80 (■) treated with cytochalasin B compared with 37 °C without inhibition (100% uptake).

be involved in the SLN internalisation. The main uptake pathway seems to be the clathrin mediated endocytosis, but for some cells (A172 and U87) macropinocytosis seems also to be involved in this process, but to a smaller extent.

4. Discussion

The key physicochemical parameters of nanoparticles that determine cellular entry of nanomedicines through endocytic routes are charge, shape, size, flexibility, material composition, coating and surface chemistry (Sahay et al., 2010). It has long been believed that the size of nanoparticles may play a paramount role in their inclusion within different endocytic vesicles that greatly vary in size. Furthermore, particles sizing in the range below 200 nm has been reported as potentially longer circulating whereas particles smaller than 30 nm are eliminated by renal excretion, and larger can be rapidly taken up by the MPS cells (Moghimi et al., 2001; Gaumet et al., 2008).

The mean diameter of the SLN produced (~135–165 nm) seems to be suitable for reaching cancer cells and to be taken up by these cells. Despite that a small size (<200 nm) may be beneficial for a rapid entry into cells, there is no size cut off limit up to at least 5 μm to gain cellular entry of some materials through pinocytosis. The largest particles may be more likely to enter cells through macropinocytosis. The size of the particles may play a minor role in defining the entry pathway, than the chemical composition of the nanoparticles (Huang et al., 2002; Sahay et al., 2010).

Furthermore, tumour vasculature is immature, allowing nanoparticles to leak from the blood to accumulate in the interstitial space in tumour tissues, a phenomenon known as "enhanced permeability and retention (EPR) effect" (Torchilin, 2010). Experiments with animal models suggest that small (<200 nm), neutral or slightly negatively charged particles can move through tumour tissue (Nomura et al., 1998).

With respect to the surface charge, unloaded and R123-loaded SLN had slightly negative charge. The incorporation of the positively charged R123 did not increase but slightly decreased the zeta potential of the SLN, which is an indication that R123 is not on the surface of the SLN but mainly incorporated in the SLN lipid matrix. These negative zeta potential values are good indications

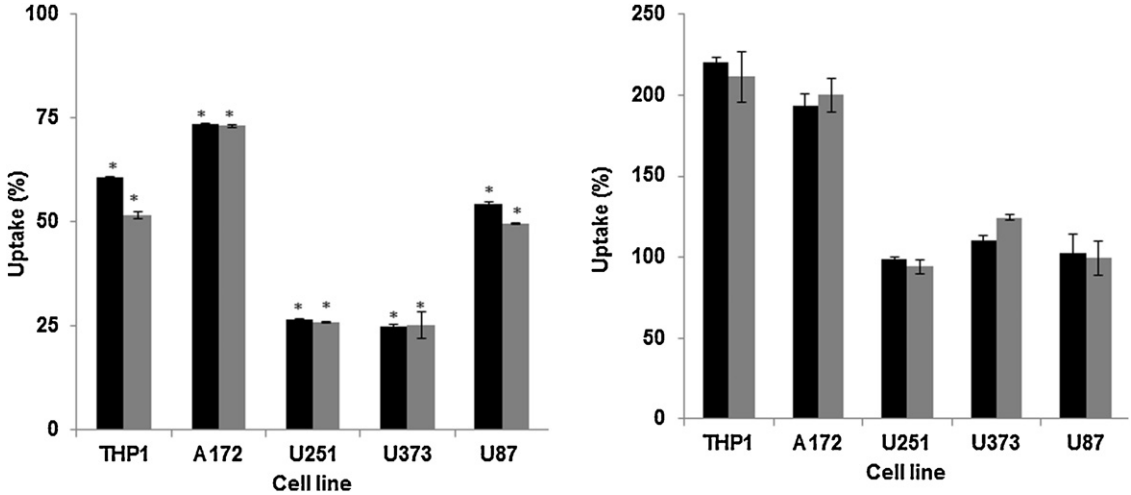

Fig. 10. Endocytosis mechanism on rhodamine 123 (R123)-loaded solid lipid nanoparticles (SLN) internalisation (fluorescence mean ± SD). Effect of clathrin-(A) and caveolae-(B) mediated endocytosis inhibition on Rh123-loaded SLN internalisation. Cells were pretreated with sucrose 0.45 M (A) or filipin (5 μg/mL) (B) during 30 min and then treated with 50 μg/mL of R123-loaded SLN stabilised with polysorbate 60 (R123-CP60, ■) and 80 (R123-CP80, ■). Subsequent analysis by flow cytometry showed a significant decrease in fluorescence for all cells treated with sucrose 0.45 M (A) but not for cells treated with filipin (5 μg/mL) (B) compared with 37 °C (100% uptake).

also for brain tumour targeting (Lockman et al., 2004). Another advantage of using slightly negatively charged SLN is that particles are expected to be less toxic and more stable than positively charged nanoparticles (Kedmi et al., 2010). Furthermore, Lockman et al. (Lockman et al., 2004) revealed that neutral nanoparticles (−14.1 mV) and low concentrated anionic nanoparticles (−59.5 mV) did not affect the blood-brain barrier integrity, while cationic nanoparticles disrupted the blood-brain barrier. Additionally, brain uptake rates of anionic nanoparticles were found to be higher than neutral or cationic formulations when used at the same concentrations. The authors postulated that neutral and low concentrated anionic nanoparticles can be safely used as colloidal drug delivery systems for brain targeting. In the present paper, we report the production of unloaded and R123-loaded SLN stabilised with polysorbate 60 or 80 with only slight negative charges, between −13 and −23 mV. Based on these facts, we suggest that the developed formulations with a slightly negative charge may not exert surface associated cytotoxicity and may increase the drug delivery of loaded drugs to the brain.

There are several studies in which nanoparticles have been used to deliver drugs to the brain (Gelperina et al., 2010; Ying et al., 2010; Cirpanli et al., 2011), but most of them have problems associated with toxicity, an invasive administration route or low ability to reach the target drugs. SLN could be a safe and easy drug delivery system to overtake common problems of brain delivery, due to the low acute and chronic toxicity associated to the lipid matrix, in addition to their ability to target drugs to the brain.

DSC studies were performed to investigate the physical state, the presence of polymorphic forms and the degree of crystallinity of the SLN.

The thermograms of both formulations were quite alike due to the fact that both the melting and crystallisation properties of the SLN were mainly governed by the hard fat component than by the surfactant (Schubert and Muller-Goymann, 2005; Bunjes and Unruh, 2007).

According to the literature, the bulk cetyl palmitate exists in two different polymorphic or crystalline forms: α form (meta-stable) and β form (stable form) (Saupe et al., 2005). The decrease of the onset temperature and the melting peak of the SLN comparing to the bulk materials (4–7 °C) can be explained by the presence of a surfactant, the small diameters of the colloidal dispersion and their high surface area (Bunjes et al., 2000, 2003). The reduction in crystallinity is due to the partial formation of lower energy lipid forms (lower ordered lattice arrangement). In addition, surfactants distributed in the melted lipid phase can distort crystallisation, resulting in a lower melting enthalpy.

Although crystalline lipids are used for the production of SLN dispersions, the lipid particles are not necessarily present in the solid state after processing (Kuntsche and Bunjes, 2007). Consequently, reassuring the physical state of the matrix lipid is of utmost relevance for the development of nanoparticles based on solid lipids. Thermograms revealed that cetyl palmitate-based SLN have melting temperatures much higher than 40 °C which is sufficient to consider that the lipids are in the solid state at both room and body temperature.

In vitro cytotoxicity studies (MTT) revealed that the cells exposed to the high SLN concentrations tested (50 μg/mL to 0.5 mg/mL) for the 24 h were not affected in the same way. In fact, SLN were more toxic to the glioma cells than to macrophages. These results revealed a higher biocompatibility of the SLN with the normal human macrophages cells than with human cancer cells (gliomas). This selective toxicity for cancer cells could be used combined with other anticancer drugs in the treatment of neoplastic diseases, such as brain tumours. Literature indicates however that at lower concentration, SLN are generally well tolerated for several cell lines (Schöler et al., 2000; Nassimi et al., 2010; Silva et al., 2011).

Complementary to the MTT cytotoxicity studies, the *in vitro* studies of flow cytometry revealed that the SLN and the excluded endocytosis conditions used were not toxic (viability higher than 90%) for all the cells during the time (2 h) of the internalisation *in vitro* experiments, which are required for a better analysis of the endocytosis pathway (data not shown).

In this work we studied the amount of internalisation of SLN stabilised with two different surfactants (polysorbate 60 and 80) and the different pathways that may be responsible for SLN uptake.

Fluorescence microscopy and flow cytometry analysis showed a remarkable intracellular localisation of both formulations in all the four glioma cell lines and slightly less in the macrophages after 2 h of exposition to both R123-loaded SLN formulations (Figs. 3 and 6).

Internalisation of SLN stabilised with polysorbate 60 or 80 were similar suggesting similar uptake of the SLN by all the cells. Furthermore, the internalisation of both formulations was higher (at least two times higher) for all the glioma cell lines than for macrophages. However, these differences were significant only for A172 and U87 cell lines. For the U251 and U373 there are no significant differences possibly due to the fact that these experiments are associated intrinsically with high SD which decreases the significant differences between groups.

For any drug delivery system, understanding the initial mode of internalisation is the first step in achieving optimised drug delivery. For the 5 cell lines R123-CP60 and R123-CP80 endocytosis was strongly inhibited in all cells by lowered temperatures. This is consistent with previous studies from the literature (Kam et al., 2006; Thurn et al., 2011) indicating that cargo uptake is usually energy-dependent. Subcellular internalisation of R123-loaded SLN predominantly takes place by energy dependent endocytosis.

Internalisation of nanoparticles can occur by macropinocytosis, phagocytosis, clathrin-mediated endocytosis, caveolae-mediated endocytosis, or clathrin- and caveolae-independent pathways (Conner and Schmid, 2003; Doherty and McMahon, 2009; Sahay et al., 2010).

Sucrose, a specific inhibitor of clathrin-dependent endocytosis, significantly affect SLN uptake. In contrast, filipin, a specific inhibitor of caveolae-dependent endocytosis, did not significantly reduce SLN uptake. Actually, for THP1 and A172 the internalisation was significantly increased. This fact could be explained due to an interference of filipin with the cholesterol present in the membranes and the presence of the polysorbates in the SLN surface that may in addition increase cell membrane fluidity, leading to endocytosis activation (Kam et al., 2006; Sahay et al., 2010; Tahara et al., 2010).

Clathrin-mediated endocytosis was significantly inhibited in all cell lines. These data suggest that for all cell lines the main mechanism of SLN internalisation is the endocytosis, and more specifically, endocytosis mediated by clathrin.

Macropinocytosis pathway involves internalisation of relatively large particles (1–5 μm diameter), much larger than the SLN produced, with sizes lower than 200 nm. Phagocytosis is usually associated with specialised cells (Khalil et al., 2006), however some epithelial cells are also capable of it (Mayerson and Hall, 1986). Nevertheless, we found that the phagocytosis/macropinocytosis of the four human glioma cell lines *in vitro* was negligible or reduced (A172 and U87). For the A172 and U87 cells appears that the endocytosis could occur by more than one pathway (clathrin-mediated endocytosis and macropinocytosis).

These findings suggest that SLN are mainly internalised by the clathrin-mediated endocytosis pathway.

5. Conclusion

In conclusion, we have shown that SLN stabilised with two different surfactants (polysorbate 60 and 80) were capable of the

transportation of the model drug (R123) into living cells and that the cellular-uptake mechanism is energy-dependent endocytosis. The internalisation was higher in glioma than in the macrophage cell lines which could be favourable in case of brain tumours.

The detailed endocytosis pathway for the developed SLN was mostly through clathrin-coated pits rather than caveolae or lipid rafts or phagocytosis. Knowledge of the mechanism of entry is essential and will assist future developments of lipid nanoparticles for drug delivery applications.

We first showed that intracellular transportation of R123 by SLN is indeed general, thus further confirming the transporter ability of these materials. We then evidenced that clathrin-dependent endocytosis is the pathway for the uptake of various SLN with R123.

To conclude, we propose that SLN stabilised with polysorbate 60 and 80 are internalised by glioma cell lines by an energy dependent mechanism mediated mainly through a clathrin-dependent endocytic pathway. These findings further support the potential use of SLN to deliver drugs to the brain to treat brain tumours.

Declaration of interest

The authors report no declaration of interest.

Acknowledgement

This work was supported by Fundação para a Ciência e a Tecnologia (FCT), Portugal (SFRH/BD/37364/2007).

References

Blasi, P., Giovagnoli, S., Schoubben, A., Ricci, M., Rossi, C., 2007. Solid lipid nanoparticles for targeted brain drug delivery. Adv. Drug Delivery Rev. 59, 454–477.

Brandenberger, C., Muhlfeld, C., Ali, Z., Lenz, A.G., Schmid, O., Parak, W.J., Rothen-Rutishauser, B., et al., 2010. Quantitative evaluation of cellular uptake and trafficking of plain and polyethylene glycol-coated gold nanoparticles. Small 6, 1669–1678.

Brioschi, A., Zenga, F., Zara, G.P., Gasco, M.R., Ducati, A., Mauro, A., 2007. Solid lipid nanoparticles: could they help to improve the efficacy of pharmacologic treatments for brain tumors? Neurol. Res. 29, 324–330.

Brioschi, A.M., Calderoni, S., Zara, G.P., Priano, L., Gasco, M.R., Mauro, A., 2009. Chapter 11 – solid lipid nanoparticles for brain tumors therapy: state of the art and novel challenges. Prog. Brain Res. 180, 193–223.

Bunjes, H., Koch, M.H., Westesen, K., 2003. Influence of emulsifiers on the crystallization of solid lipid nanoparticles. J. Pharm. Sci. 92, 1509–1520.

Bunjes, H., Koch, M.H.J., Westesen, K., 2000. Effect of particle size on colloidal solid triglycerides. Langmuir 16, 5234–5241.

Bunjes, H., Unruh, T., 2007. Characterization of lipid nanoparticles by differential scanning calorimetry, X-ray and neutron scattering. Adv. Drug Delivery Rev. 59, 379–402.

Chen, Z., 2010. Small-molecule delivery by nanoparticles for anticancer therapy. Trends Mol. Med. 16, 594–602.

Cirpanli, Y., Allard, E., Passirani, C., Bilensoy, E., Lemaire, L., Calis, S., Benoit, J.P., 2011. Antitumoral activity of camptothecin-loaded nanoparticles in 9L rat glioma model. Int. J. Pharm. 403, 201–206.

Conner, S.D., Schmid, S.L., 2003. Regulated portals of entry into the cell. Nature 422, 37–44.

Doherty, G.J., McMahon, H.T., 2009. Mechanisms of endocytosis. Annu. Rev. Biochem. 78, 857–902.

Gaumet, M., Vargas, A., Gurny, R., Delie, F., 2008. Nanoparticles for drug delivery: the need for precision in reporting particle size parameters. Eur. J. Pharm. Biopharm. 69, 1–9.

Gelperina, S., Maksimenko, O., Khalansky, A., Vanchugova, L., Shipulo, E., Abbasova, K., Kreuter, J., et al., 2010. Drug delivery to the brain using surfactant-coated poly(lactide-co-glycolide) nanoparticles: influence of the formulation parameters. Eur. J. Pharm. Biopharm. 74, 157–163.

Hillaireau, H., Couvreur, P., 2009. Nanocarriers' entry into the cell: relevance to drug delivery. Cell. Mol. Life Sci. 66, 2873–2896.

Huang, M., Ma, Z., Khor, E., Lim, L.Y., 2002. Uptake of FITC-chitosan nanoparticles by A549 cells. Pharm. Res. 19, 1488–1494.

Jain, A., Agarwal, A., Majumder, S., Lariya, N., Khaya, A., Agrawal, H., Agrawal, G.P., et al., 2010. Mannosylated solid lipid nanoparticles as vectors for site-specific delivery of an anti-cancer drug. J. Controlled Release 148, 359–367.

Joshi, M.D., Müller, R.H., 2009. Lipid nanoparticles for parenteral delivery of actives. Eur. J. Pharm. Biopharm. 71, 161–172.

Kam, N.W.S., Liu, Z., Dai, H., 2006. Carbon nanotubes as intracellular transporters for proteins and dna: an investigation of the uptake mechanism and pathway. Angew. Chem. Int. Ed. 45, 577–581.

Kaur, I.P., Bhandari, R., Bhandari, S., Kakkar, V., 2008. Potential of solid lipid nanoparticles in brain targeting. J. Controlled Release 127, 97–109.

Kedmi, R., Ben-Arie, N., Peer, D., 2010. The systemic toxicity of positively charged lipid nanoparticles and the role of Toll-like receptor 4 in immune activation. Biomaterials 31, 6867–6875.

Khalil, I.A., Kogure, K., Akita, H., Harashima, H., 2006. Uptake pathways and subsequent intracellular trafficking in nonviral gene delivery. Pharmacol. Rev. 58, 32–45.

Kuntsche, J., Bunjes, H., 2007. Influence of preparation conditions and heat treatment on the properties of supercooled smectic cholesteryl myristate nanoparticles. Eur. J. Pharm. Biopharm. 67, 612–620.

Kuo, Y.C., Liang, C.T., 2011. Inhibition of human brain malignant glioblastoma cells using carmustine-loaded catanionic solid lipid nanoparticles with surface anti-epithelial growth factor receptor. Biomaterials 32, 3340–3350.

Lai, S.K., Hida, K., Man, S.T., Chen, C., Machamer, C., Schroer, T.A., Hanes, J., 2007. Privileged delivery of polymer nanoparticles to the perinuclear region of live cells via a non-clathrin, non-degradative pathway. Biomaterials 28, 2876–2884.

Lockman, P.R., Koziara, J.M., Mumper, R.J., Allen, D.D., 2004. Nanoparticle surface charges alter blood-brain barrier integrity and permeability. J. Drug Target 12, 635–641.

Mayerson, P.L., Hall, M.O., 1986. Rat retinal pigment epithelial cells show specificity of phagocytosis *in vitro*. J. Cell Biol. 103, 299–308.

Moghimi, S.M., Hunter, A.C., Murray, J.C., 2001. Long-circulating and target-specific nanoparticles: theory to practice. Pharmacol. Rev. 53, 283–318.

Mosmann, T., 1983. Rapid colorimetric assay for cellular growth and survival: application to proliferation and cytotoxicity assays. J. Immunol. Methods 65, 55–63.

Nassimi, M., Schleh, C., Lauenstein, H.D., Hussein, R., Hoymann, H.G., Koch, W., Müller-Goymann, C., et al., 2010. A toxicological evaluation of inhaled solid lipid nanoparticles used as a potential drug delivery system for the lung. Eur. J. Pharm. Biopharm. 75, 107–116.

Nomura, T., Koreeda, N., Yamashita, F., Takakura, Y., Hashida, M., 1998. Effect of particle size and charge on the disposition of lipid carriers after intratumoral injection into tissue-isolated tumors. Pharm. Res. 15, 128–132.

Sahay, G., Alakhova, D.Y., Kabanov, A.V., 2010. Endocytosis of nanomedicines. J. Controlled Release 145, 182–195.

Saupe, A., Wissing, S.A., Lenk, A., Schmidt, C., Muller, R.H., 2005. Solid lipid nanoparticles (SLN) and nanostructured lipid carriers (NLC) - structural investigations on two different carrier systems. Biomed. Mater. Eng. 15, 393–402.

Schöler, N., Zimmermann, E., Katzfey, U., Hahn, H., Müller, R.H., Liesenfeld, O., 2000. Preserved solid lipid nanoparticles (SLN) at low concentrations do cause neither direct nor indirect cytotoxic effects in peritoneal macrophages. Int. J. Pharm. 196, 235–239.

Schubert, M.A., Muller-Goymann, C.C., 2005. Characterisation of surface-modified solid lipid nanoparticles (SLN): influence of lecithin and nonionic emulsifier. Eur. J. Pharm. Biopharm. 61, 77–86.

Serda, R.E., Gu, J., Bhavane, R.C., Liu, X., Chiappini, C., Decuzzi, P., Ferrari, M., 2009. The association of silicon microparticles with endothelial cells in drug delivery to the vasculature. Biomaterials 30, 2440–2448.

Silva, A.C., González-Mira, E., García, M.L., Egea, M.A., Fonseca, J., Silva, R., Ferreira, D., et al., 2011. Preparation, characterization and biocompatibility studies on risperidone-loaded solid lipid nanoparticles (SLN): high pressure homogenization versus ultrasound. Colloid Surf. B 86, 158–165.

Souto, E.B., Muller, R.H., 2010. Lipid nanoparticles: effect on bioavailability and pharmacokinetic changes. Handb. Exp. Pharmacol., 115–141.

Stupp, R., Hegi, M.E., van den Bent, M.J., Mason, W.P., Weller, M., Mirimanoff, R.O., Cairncross, J.G., 2006. Changing paradigms-an update on the multidisciplinary management of malignant glioma. Oncologist 11, 165–180.

Sugano, M., Egilmez, N.K., Yokota, S.J., Chen, F.A., Harding, J., Huang, S.K., Bankert, R.B., 2000. Antibody targeting of doxorubicin-loaded liposomes suppresses the growth and metastatic spread of established human lung tumor xenografts in severe combined immunodeficient mice. Cancer Res. 60, 6942–6949.

Tahara, K., Yamamoto, H., Kawashima, Y., 2010. Cellular uptake mechanisms and intracellular distributions of polysorbate 80-modified poly (d,l-lactide-co-glycolide) nanospheres for gene delivery. Eur. J. Pharm. Biopharm. 75, 218–224.

Thurn, K., Brown, E., Wu, A., Vogt, S., Lai, B., Maser, J., Woloschak, G., et al., 2007. Nanoparticles for applications in cellular imaging. Nanoscale Res. Lett. 2, 430–441.

Thurn, K.T., Arora, H., Paunesku, T., Wu, A., Brown, E.M.B., Doty, C., Woloschak, G., et al., 2011. Endocytosis of titanium dioxide nanoparticles in prostate cancer PC-3M cells. Nanomed. Nanotechnol. Biol. Med. 7, 123–130.

Torchilin, V.P., 2010. Passive and active drug targeting: drug delivery to tumors as an example. Handb. Exp. Pharmacol., 3–53.

Westphal, M., Hilt, D., Bortey, E., Delavault, P., Olivares, R., Warnke, P., Ram, Z., et al., 2003. A phase 3 trial of local chemotherapy with biodegradable carmustine (BCNU) wafers (Gliadel wafers) in patients with primary malignant glioma. Neuro Oncol. 5, 79–88.

Ying, X., Wen, H., Lu, W.L., Du, J., Guo, J., Tian, W., Zhang, Q., et al., 2010. Dual-targeting daunorubicin liposomes improve the therapeutic efficacy of brain glioma in animals. J. Controlled Release 141, 183–192.